We are IntechOpen,
the world's leading publisher of
Open Access books
Built by scientists, for scientists

6,900
Open access books available

185,000
International authors and editors

200M
Downloads

154
Countries delivered to

Our authors are among the

TOP 1%
most cited scientists

12.2%
Contributors from top 500 universities

CLARIVATE ANALYTICS

BOOK CITATION INDEX

INDEXED

WEB OF SCIENCE™

Selection of our books indexed in the Book Citation Index
in Web of Science™ Core Collection (BKCI)

Interested in publishing with us?
Contact book.department@intechopen.com

Numbers displayed above are based on latest data collected.
For more information visit www.intechopen.com

Intra-Cavity Nonlinear Frequency Conversion with Cr³⁺-Colquiriite Solid-State Lasers

H. Maestre, A. J. Torregrosa and J. Capmany
Photonic Systems Group, Universidad Miguel Hernández
Elche, Alicante,
Spain

1. Introduction

The availability of laser radiation in new wavelengths is a research topic of permanent interest. Nonlinear optical frequency conversion of a primary laser radiation is one of the widely exploited resources for this purpose. Since the birth of nonlinear optics with the first demonstration of second harmonic generation of laser radiation, new ways and new materials are seek. Due to the inherent low conversion efficiency of nonlinear optical mixing related to the decreasing efficiency of higher order terms in the nonlinear Taylor expansion of the optical polarization with the electric field, second-order nonlinear optics referred to as three-wave mixing processes is in general preferred. It is well stated that nonlinear optical frequency conversion efficiency improves with increasing power density –and thus amplitude- of the primary optical field, material nonlinear response and interaction length as well as with providing a suitable phase relation among the interacting electromagnetic waves (Armstrong et al., 1962). It was soon realized that conversion of pulsed lasers that emit high peak power pulses could result efficient in a simple manner, by just single-passing the interacting waves through a suitable nonlinear medium, generally an anisotropic crystal.

The case of continuous-wave is more challenging due to the lower peak power available in comparison with pulsed lasers. A skilled technique –intracavity conversion-, where the nonlinear crystal is placed inside the cavity of the primary laser, was developed as a way to boost conversion efficiency in the continuous-wave case, particularly in case of solid-state lasers. Because the circulating intracavity power is typically around two orders of magnitude higher than in the output of a solid-state laser where typical optimal output coupling is achieved with a few percent transmission, a rough estimation of the power circulating inside the cavity is given by $P_{intra} \approx \frac{P_{out}}{T}$ with $T \approx 0.02 - 0.06$. As a result, a small fraction of intracavity conversion can provide an amount of useful converted power that equals the primary laser output in the absence of any conversion. The key for efficient intracavity conversion resides in confining as much as possible the primary laser within the cavity and to provide its output coupling through conversion of energy to another wavelength rather than by an outcoupling mirror (Smith, 1970).

Early intracavity nonlinear conversion focused on realizing a single conversion process like SHG or SFM in the primary laser, based on perfect phase matching in birefringent nonlinear

crystals. A very useful alternative to phase matching is quasiphase matching based on domain-engineered nonlinear ferroelectric crystal. With quasiphase matching more than one nonlinear interaction (conversion) can be realized simultaneously in the same physical nonlinear crystal. A high degree of flexibility for the generation of new wavelengths can be achieved when the primary laser can oscillate simultaneously in different wavelengths and the nonlinear crystal can realize several different nonlinear conversion processes among those wavelengths. For this reason, gain materials with a broad gain bandwidth combined with a domain-engineered ferroelectric crystal become particularly useful.

Cr^{3+}-doped colquiriites can provide tunable lasing in a wide spectral range around 750-950 nm much like the well-established Ti^{3+}-Sapphire laser. However, Cr^{3+}-doped colquiriites have the practical advantage of diode laser pumping with red diodes around 660-690 nm. It is worth mentioning that the use of these lasers in intracavity nonlinear frequency generation has been little explored so far. Throughout this chapter it is intended to show the potential of these systems in the 1500-1700 nm spectral band. For this aim, the characteristics of chromium-doped colquiriite crystals are described firstly. Next, a description of the basic physics involving second-order nonlinear interactions is presented, where the allowed processes for three-wave mixing are detailed. Due to the dispersion of nonlinear media, a review of techniques for controlling the phase-matching among interacting waves is made, paying special attention to the flexibility and versatility offered by quasi-phase matching (QPM) in periodically poled ferroelectric crystals. Coherent radiation by intracavity wavelength conversion is described from the inclusion of such nonlinear crystals inside the resonator of a Cr-doped colquiriite lasers. Before conclusions, some examples of wavelength converting systems based on optical parametric oscillation and difference frequency generation are reported.

2. Characteristics of Cr^{3+}-doped colquiriite crystals

Cr^{3+} is one of the most popular ions used in inorganic solid-state lasers. It was also employed as the optical gain material in the first experimental demonstration of lasing action conducted by T. H. Maiman in 1960 (ruby laser) (Maiman, 1960). It is usually included in the group of transition metal lasers.

2.1 Chromium doped laser crystals

Crystals for solid-state lasers based on such ion are made of host materials containing aluminium. During growth of the crystal, some amount of Al^{3+} ions is replaced with Cr^{3+} ions and, therefore, a Cr^{3+}-doped crystal is obtained. Depending on the host, the intensity of the crystal electric field varies and, thus, Cr^{3+} ions are affected in a different manner by different hosts. The crystal electric field perturbs, among other properties, optical properties of the laser ion (energy levels, absorption, stimulated cross section, radiative and non-radiative lifetimes, transition linewidth, etc…). A high crystal field intensity induces narrow emission linewidths (as in ruby lasers), a moderate crystal field intensity allows both narrow and broad emission linewidths (as in alexandrite laser), whereas in a low intensity crystal electric field a broad emission linewidth is obtained, which is desirable for tunable lasers and characteristic of colquiriite (fluoride) lasers. Typical and well-known colquiriite host materials are $LiCaAlF_6$ (LiCAF) (Payne et al., 1988), $LiSrAlF_6$ (LiSAF) (Payne et al., 1989) and $LiSrGaAlF_6$ (LiSGAF) (Smith et al., 1992).

2.2 Energy levels, absorption and stimulated emission in Cr³⁺-doped colquiriites

Cr³⁺-doped colquiriites belong to the family of lasers called vibronic lasers. In such laser gain media exist a strong interaction of the electronic states with lattice vibrations (phonons). This vibrational–electronic interaction leads to a pronounced homogeneous broadening and thus to a broad optical gain bandwidth. There are four main energy levels in Cr³⁺ ions ($^4T_1$, $^4T_2$, ^2E and $^4A_2$) as it is shown in Fig. 1.
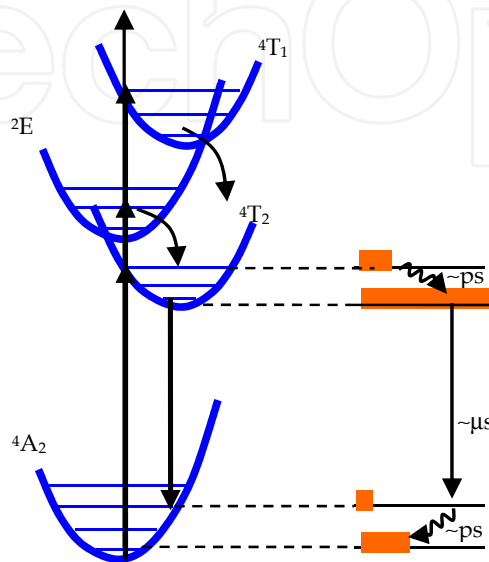

Fig. 1. Cr³⁺ ion energy levels in colquiriites.

Due to the electric forces acting on Cr³⁺ ion and in contrast to other Cr³⁺-doped media, in Cr³⁺-colquiriites the ^2E energy level lays above the $^4T_2$ and below the $^4T_1$ levels respectively. In these crystals the absorption and thus the channels allowing direct laser pumping are due to transitions between the $^4A_2$ ground state and ^2E or $^4T_1$ upper states ($^4A_2 \rightarrow {}^2E$ or $^4A_2 \rightarrow {}^4T_1$). At room temperature the $^4A_2 \rightarrow {}^2E$ transition can be pumped by means of commercially available red light diode lasers. The electrons excited to the ^2E state decay rapidly in a non-radiative fashion to the $^4T_2$ state, becoming the latter the most populated level and hence the upper laser level. Radiative rate from $^4T_2 \rightarrow {}^4A_2$ (much greater than that from $^2E \rightarrow {}^4A_2$) gives rise to stimulated emission in a four-level like laser system. Depending on the colquiriite host crystal, different stimulated emission peaks and tuning ranges can be obtained. As examples and for a higher detail on absorption and emission bands, Cr:LiSAF and Cr:LiCAF are shown in figures 2.a and 2.b respectively. Since colquiriites are uniaxial crystals, Cr³⁺ emission and absorption in such materials is strongly polarization dependant (parallel to c-axis (π-polarization) and perpendicular to c-axis (σ-polarization)).

As it can be seen Cr:LiSAF and Cr:LiCAF have quite similar absorption spectra but main differences arise from the emission spectra. Absorption peaks and the relative strengths of the peaks occur at nearly the same wavelengths and have similar values but, nevertheless, absolute absorption strengths for Cr:LiSAF are roughly twice as strong as those of Cr:LiCAF. Strongest absorption peaks for the π-polarization are approximately at 0.425 and 0.630 μm. Strongest absorption peaks for the σ-polarization are approximately at 0.423 and 0.622 μm. The absorption peak for wavelengths above 500 nm is stronger for the π-

polarization whereas the peaks for wavelengths below 500 nm are stronger for the σ-polarization. Emission from Cr:LiSAF , has a maximum emission peak at about 840 nm and a linewidth of about 197 nm for both polarizations and the π-polarized emission spectrum is approxim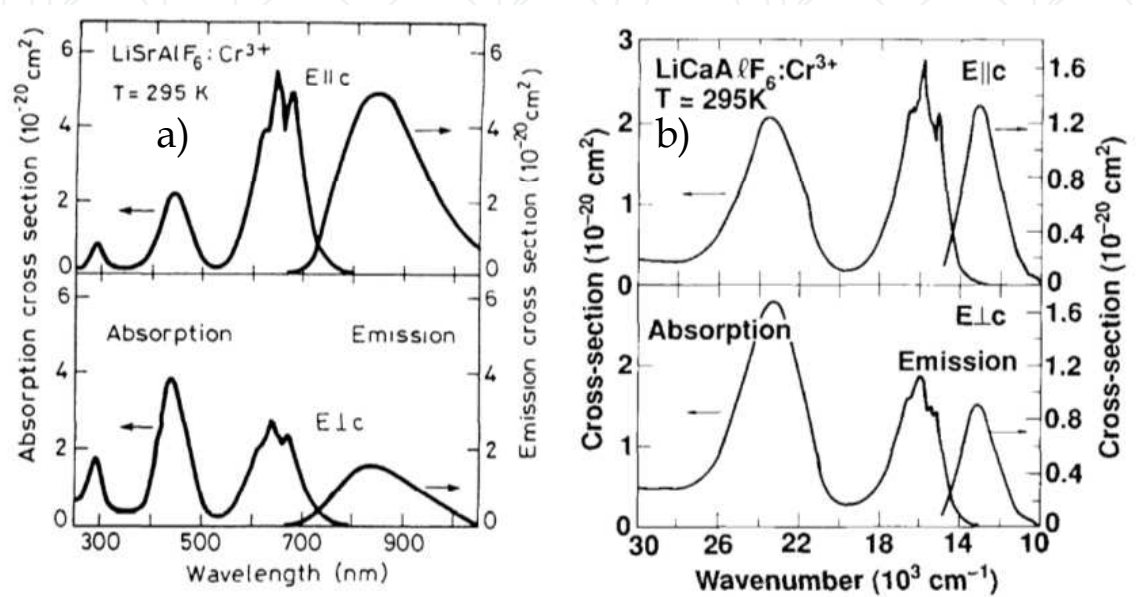ately 3 times more intense than the σ-polarized emission. On the other hand, emission from Cr:LiCaF has a maximum peak at about 775 nm and a linewidth of about 132 nm for both polarizations and the π-polarized emission is approximately 1.5 times more intense than the σ-polarized.

Fig. 2. Cr^{3+} absorption and emission cross-section spectra in a) LiSAF (Reprinted by permission from (Payne et al., 1989), American Institute of Physics) and b) LiCAF hosts (Reprinted by permission from (Payne et al., 1988), Institute of Electrical and Electronics Engineers (IEEE)).

2.3 Ti:Sapphire vs. Cr^{3+}-doped colquiriites

Cr^{3+}-doped colquiriites can be viewed as promising alternatives to titanium sapphire (Ti:Sapphire) lasers. Cr^{3+} doped fluorides (colquiriites) such as Cr^{3+}:LiSAF, Cr^{3+}:LiSGaF, and Cr^{3+}:LiCAF, belonging to solid-state vibronic lasers, can provide broadly tunable operation, high intrinsic slope efficiencies (>50%) and enable efficient laser operation with electrical-to-optical conversion efficiencies exceeding 10% (Demirbas et al., 2009). The main laser parameters are summarized in Table 1. Their peak emission cross section and their absorption bands are placed around 800 nm and 650 nm respectively, allowing direct diode pumping with commercially available AlGaInAs diode lasers around 670 nm, significantly reducing the total cost of the laser system.

In contrast to this, Ti:Sapphire lasers are typically pumped by argon gas lasers or frequency-doubled diode pumped neodymium lasers, since high power direct diode pumping is not currently available, which are bulky and thus making the overall system cost high and limiting wide-spread use. In addition, their anisotropic character readily allows polarized laser oscillation without additional polarizing elements or Brewster angle operation.

Gain material	Ti^{3+}:Al$_2$O$_3$	Cr^{3+}:LiSrAlF$_6$	Cr^{3+}:LiCaAlF$_6$	Cr^{3+}:LiSrGaAlF$_6$
Tuning range (nm)	660-1180	782-1042	754-871	777-977
Cross-section (σ_{em}) [x10^{-20} cm^2]	41	4.8	1.3	3.3
Room-temperature fluorescence lifetime (τ_f) [μs]	3.2	67	175	88
$\sigma_{em} \cdot \tau_f$ [10^{-20}xcm^{2}x μs]	131	322	228	290
Efficiency [%]	64	54	69	60
Thermal conductivity [W/k·m]	28	3.1	5.1	3.6
T$_{1/2}$, τ_f(T$_{1/2}$)=0.5·τ_{rad}	100	69	255	88
Refractive index	1.76	1.4	1.39	1.4

Table 1. Comparison of important laser parameters of the Ti:Sapphire, Cr:LiSAF, Cr:LiSGaF, and Cr:LiCAF gain media (Payne et al., 1988; Payne et al., 1989; Smith et al., 1992; Demirbas et al., 2009).

Among Cr^{3+}-doped colquiriites and despite the lower emission cross section of Cr:LiCAF as compared to other colquiriites, it offers the longest fluorescence lifetime and a high thermal conductivity, which reduces thermal lensing effects caused by high power pumping and preserves a good-quality mode when scaling power. Moreover, Cr:LiCAF suffers lower quantum defect due its blue shifted emission spectrum, as well as lower excited-state absorption (ESA) and upconversion rate (Eichenholz and Richardson, 1998).

3. Nonlinear optics and materials

In conventional (linear) optics, the interaction between an electro-magnetic wave and a dielectric material results in an induced polarization of the material which depends linearly upon the incident electric field. In non linear optical materials, the relation between the induced polarization and the incident electric field is no longer linear and can be described by means of a power series expansion of the electric susceptibility (equation (1)).

$$P_i(t) = \varepsilon_0 \chi_{ij}^{(1)} E_j(t) + \varepsilon_0 \chi_{ijk}^{(2)} E_j(t) E_k(t) + \varepsilon_0 \chi_{ijkl}^{(3)} E_j(t) E_k(t) E_l(t) + \dots \tag{1}$$

The first-order term of the expansion gives rise to linear optics effects (refractive index, reflection, refraction, dispersion…) whereas higher order terms of the expansion (such as $\chi_{ijk}^{(2)}$ or $\chi_{ijkl}^{(3)}$) give rise to nonlinear effects which are responsible of the generation of new frequencies other than that of the incident wave. Such terms are tensors relating electric fields of same or different frequency and polarization to the optically induced nonlinear polarization. If the incident wave intensity is strong enough, the terms $\chi_{ijk}^{(2)}$ and $\chi_{ijkl}^{(3)}$ lead to second and third-order nonlinear effects respectively. In the following sections we will focus on second-order nonlinear processes.

3.1 Second-order nonlinear processes

Optical nonlinear second-order processes are determined by the second term ($\chi^{(2)}$) of the optical susceptibility series expansion or the more extensively used nonlinear coefficient $d = \frac{1}{2}\chi^{(2)}_{ijk}$ Such processes may be regarded as the interaction of one photon of frequency ω_1 and wavenumber k_1 combining with other photon of frequency ω_2 and wavenumber k_2 to yield a third photon of frequency ω_3 and wavenumber k_3. Allowed processes for three-wave mixing of continuous-wave (CW) signals are represented in Fig. 3: second-harmonic generation (SHG), sum-frequency generation (SFG), difference frequency generation (DFG), optical parametric generation (OPG), optical parametric amplification (OPA) and optical parametric oscillation (OPO).
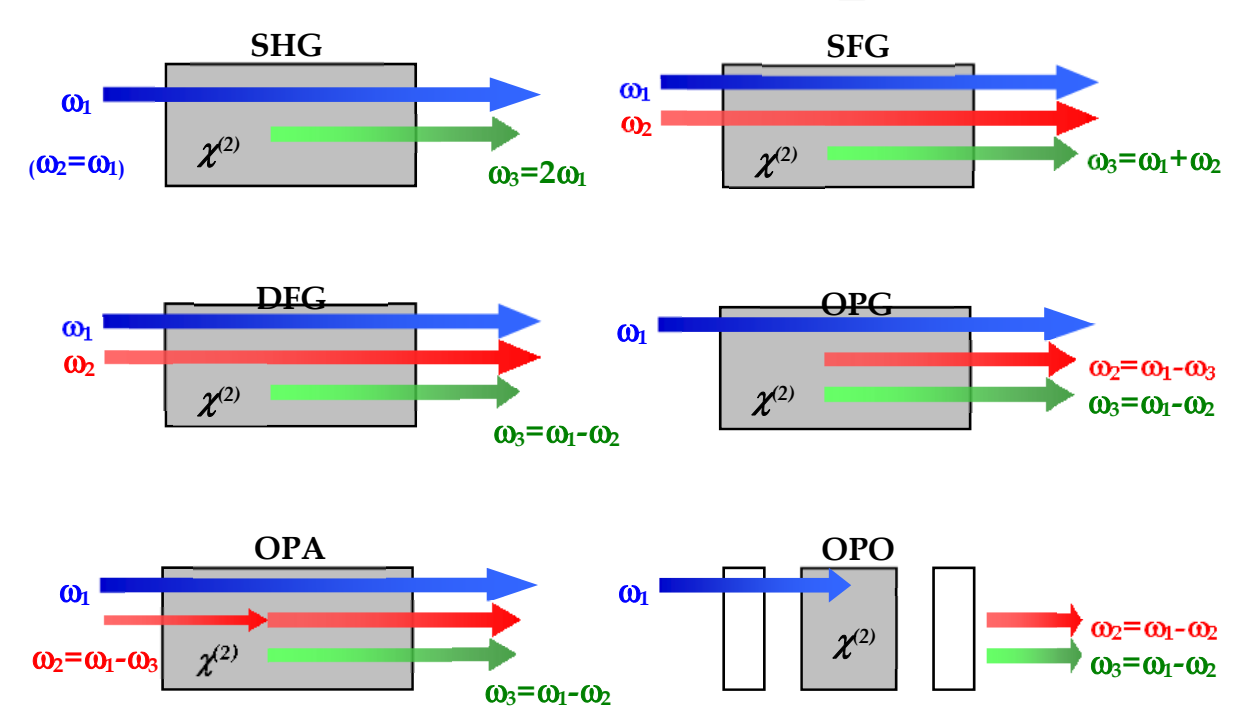
Fig. 3. Interacting waves and different second-order nonlinear optical processes.

In order to select a nonlinear process and to obtain efficient non linear interactions, it is necessary to fulfill both the photon energy, equation (2.a), and momentum conservation along the non linear crystal length. The momentum conservation condition is also known as the phase-matching condition. The phase-matching condition is represented in equation (2.b) where the l, m and n subscripts stand for the higher and lower frequency interacting waves respectively.

$$\omega_l = \omega_m + \omega_n \qquad (2a)$$

$$k_l = k_m + k_n \rightarrow \frac{\omega_l}{c}n(\omega_l) = \frac{\omega_m}{c}n(\omega_m) + \frac{\omega_n}{c}n(\omega_n) \qquad (2b)$$

The conversion efficiency, i.e. the amount of incoming power converted into a different frequency, is proportional to the square of effective nonlinear coefficient d_{eff} (the nonlinear

coefficient for a given propagation direction and polarization of waves in the crystal), crystal length L, and the phase mismatch Δk in through the term $sinc^2(\Delta kL/2)$ (equation (3)). It is difficult to meet the phase-matching condition due to dispersion of the refractive index. If the phase-matching condition is not completely fulfilled a phase mismatch $\Delta k = k_l - k_m - k_n \neq 0$ is obtained and crystal length L is limited to the coherence length, i.e. $l_c = \pi/\Delta k$, thus reducing the conversion efficiency.

$$\eta \equiv \frac{P_{converted}}{P_{incident}} \propto d_{eff}^2 \frac{\sin^2(\Delta kL/2)}{(\Delta kL/2)^2} L^2 = d_{eff}^2 \operatorname{sinc}^2(\Delta kL/2)L^2 \tag{3}$$

As a result, it is important to operate as close as possible to the condition $\Delta k = 0$. We will discuss briefly two of the most employed phase-matching techniques; Birefringent Phase-Matching (BPM) and Quasi-Phase-Matching (QPM).

3.2 Birefringent phase-matching (BPM)

As it can be seen from equation 2.b, for a targeted optical nonlinear process (i.e. a given energy conservation condition) refractive indices play an important role in achieving the phase-matching condition ($\Delta k = 0$). In this respect the birefringence inherent in many nonlinear materials can be used to compensate refractive index dispersion and obtain $\Delta k = 0$.

Owing to different refractive indices for the ordinary and extraordinary electric field polarization in a birefringent crystal and for specific interacting wavelengths, the optical axis of the crystal can be oriented to a particular angle to achieve phase-matching but, nevertheless, BPM cannot enable to achieve phase-matched processes in the full transparency range of the nonlinear crystal. In addition, since BPM takes advantage of both ordinary and extraordinary polarized waves, if the extraordinary wave propagates in a direction other than that of the optical axis, the propagation direction of the extraordinary wave diverges from the propagation direction of the ordinary wave. This effect is known as walk-off and reduces the effective interaction length to the distance where ordinary and extraordinary beams do not overlap thus limiting the conversion efficiency in BPM crystals.

3.3 Quasi-phase-matching (QPM)

QPM is an alternative method to achieve phase-matching in which the sign of the nonlinear susceptibility $\chi^{(2)}$ is corrected (or modulated) at regular intervals along the propagation length of the interacting waves inside the crystal. Because of dispersion of the refractive index, the interacting waves have different phase velocities and a phase-mismatch $\Delta k \neq 0$ results. From a coupled-wave equation analysis the energy transfer between the interacting waves as they propagate through the crystal coordinate z varies as $\exp(-j\Delta kz)$ and due to the periodicity of the complex exponential function the nonlinear conversion efficiency shows an oscillatory behavior with period $l_c = \pi/\Delta k$ and thus the converted power increases and diminishes periodically with (Fig. 4, curve a). In contrast, if a perfect phase-matching condition $\Delta k = 0$ can be obtained, i.e. by using BPM, the converted power increases monotonically (Fig. 4, curve b). Even if there is a phase-mismatch $\Delta k \neq 0$, it is possible to invert the sign of the nonlinear susceptibility every coherence length and the converted power can be made to increase monotonically as well (Fig. 4, curve c).
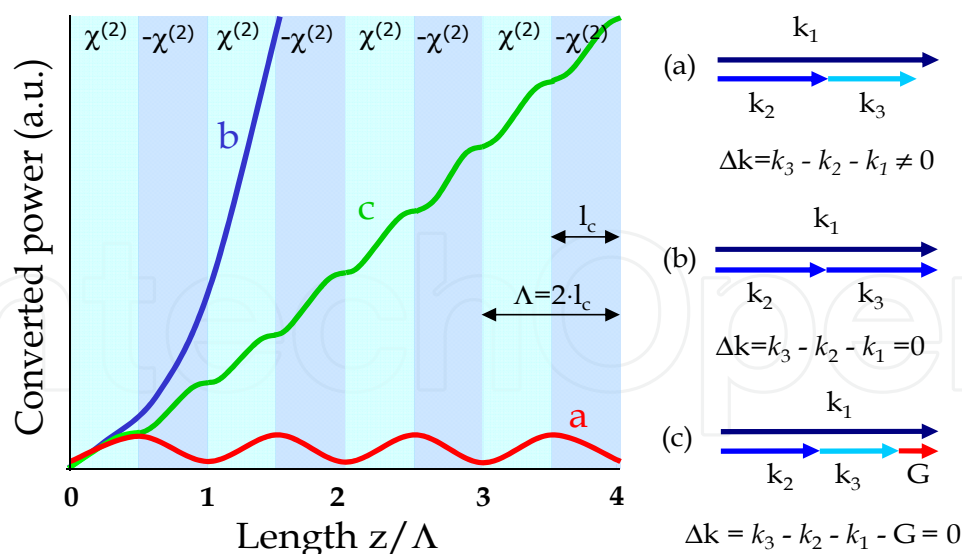
Fig. 4. Example of nonlinear converted power and wave vector mismatch for a) no phase-matching, b) BPM and c) QPM.

This is the case of QPM, where the wave vector associated with a periodic modulation of the sign of the optical susceptibility ($G=2\pi/\Lambda$) compensates for the wave vector mismatch of the interacting waves. It is important to remark that after some propagation length the converted power for QPM equals that of BPM. In contrast to BPM, QPM is not limited by walk-off (the Poynting vector is in the same direction for all interacting waves) and as a consequence longer crystals can be used (the converted crystal grows quadratically with crystal length). QPM also enables exploiting the highest non linear coefficient of a given material by choosing adequate direction of propagation and polarization in comparison to BPM where propagation direction and polarization are constrained. QPM is extensively employed in ferroelectric materials since it is a relatively easy task to reverse the sign of $\chi^{(2)}$ in such materials. The spontaneous dipolar moment can be rotated under the effect of an applied external electric field and 0°-180° alternating $\chi^{(2)}$ domains can be created and such materials are known as periodically poled crystals. Most employed periodically poled crystals are lithium niobate ($LiNbO_3$, PPLN), lithium tantalate ($LiTaO_3$, PPLT), potassium-titanyl phosphate ($KTiOPO_4$, PPKTP) and potassium niobate ($KNbO_3$, PPKN).

The alternating domains result in a periodic grating that can be modeled by means of a position dependent function (Fig. 5):

$$d(z) = d_{eff}\Pi(z) \tag{4}$$

where d_{eff} is the effective nonlinear coefficient and $\Pi(z)$ is a square function of period Λ with amplitude of ± 1 (associated to opposite directions of the spontaneous polarization of ferroelectric domains) and representing the spatial distribution of domain reversals in the crystal, as it is shown in Fig. 5.

Therefore, the relative conversion efficiency associated to a collinear QPM nonlinear interaction of wavevector mismatch Δk is related to the Fourier transform $\hat{\Pi}(\Delta k)$ of the spatial distribution $\Pi(z)$:

$$\eta(\Delta k) \propto \left|\hat{\Pi}(\Delta k)\right|^2 = \left|\frac{1}{L}\int_0^L d(z)e^{-j\Delta kz}dz\right|^2 = \left|\frac{d_{eff}}{L}\int_0^L \Pi(z)e^{-j\Delta kz}dz\right|^2 \qquad (5)$$

This result enables domain engineering since periodicity can be controlled and selected to provide a phase-matched interaction for any frequency conversion process within the transparency range of the material. This means an additional advantage over BPM. In this way, the design of the domain structure is reduced to find a spatial function which describes the strategic distribution of domain reversals which produces the desired QPM spectral response (Liu et al., 2001; Pousa and Capmany, 2005).
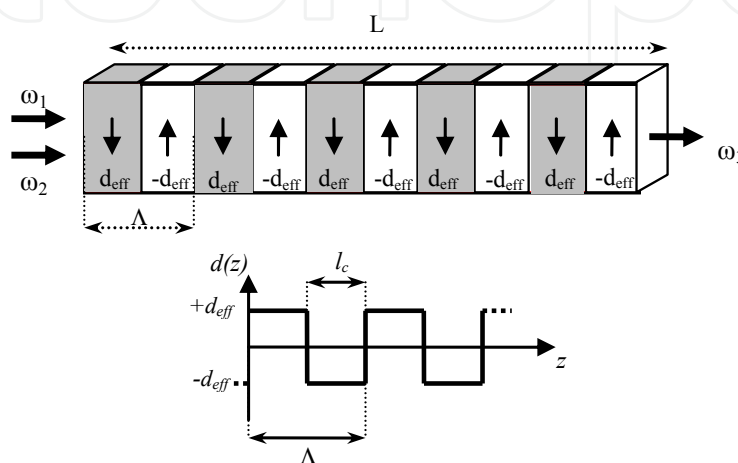
Fig. 5. Ferroelectric domain reversal and spatial distribution function in a periodically poled crystal.

Then, domain engineering permits the fabrication of ferroelectric structures which provide targeted QPM responses, consisting of a set of reciprocal vectors which participate to phase-match multiple interactions simultaneously over the same device. As QPM is sensitive to refractive index variations, the overall QPM response can be modified by altering the quasi-phase-matching condition in ferroelectric crystals through the control of the temperature (Belmonte et al., 1999) or the linear electro-optical (Pockels) effect (Xu et al., 2003). In this way, it is possible to effectively increase the number of interactions (reciprocal vectors) at the same device at no expense of nonlinearity (Torregrosa et al., 2008).

4. Intracavity nonlinear frequency conversion and external cavity lasers

As stated before, nonlinear optical frequency conversion arises only if sufficiently high optical intensities are incident to the nonlinear crystal material and becomes more pronounced as the optical intensity of the incoming waves grow higher. Usually, high optical intensities cannot be obtained from low- or moderate-power continuous-wave solid-state lasers and, as a consequence, the conversion efficiency is very low.

Since a high intensity is equivalent to a relatively high power focused to a small area, laser cavity modes are good candidates to pump nonlinear optical processes. In this sense an adequate solution is to place the nonlinear crystal within the laser resonator where the circulating power is several times higher than the output power emitted by the same laser (Fig. 6). This leads to high laser intensities (optical powers are well above 10 W and focused

to areas of radius well below 100 μm) and hence the nonlinear frequency conversion is enhanced by more than two orders of magnitude (Smith, 1970).
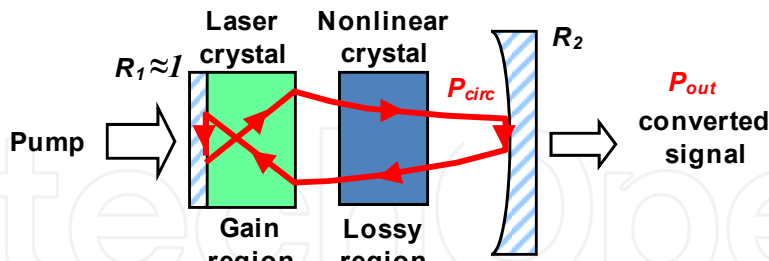

Fig. 6. Intracavity nonlinear optical conversion scheme

The power circulating inside the cavity can be approximated by $P_{circ} \approx \frac{Pout}{1-R_2}$, and, as a result, the intracavity power thus can be controlled by proper selection of the output coupler reflectivity (R_2 in Fig. 6). Careful design of the laser resonator may enhance the conversion efficiency by adjusting both size and divergence of the laser mode in the nonlinear medium (Boyd and Kleinman, 1968). Low intracavity loss due to scattering and facet reflectivity of the nonlinear crystal is desired for this type of lasers as well. If the laser emits in a multi-axial mode regime, the nonlinear medium acts as an energy exchange mechanism between them, which gives rise to noise and instabilities in the output power. In this respect, it is also interesting to operate the laser as close as possible to single-axial mode operation in order to obtain low-noise output amplitude. Furthermore, narrow-band lasers which wavelength can be tuned are highly desirable since they enable tunable optical frequency conversion owing to perturbation of the phase-matching condition.

In this regard (narrow emission linewidth and wavelength tuning capability) external-cavity solid-state lasers may play an important role. Traditionally, birefringent filters have been employed to both tune and narrow the laser emission spectrum. External-cavity solid-state lasers can be viewed as an alternative to birefringent filters because of no additional intracavity loss is produced since the tuning mechanism is not inserted within the cavity and because of their lower cost.
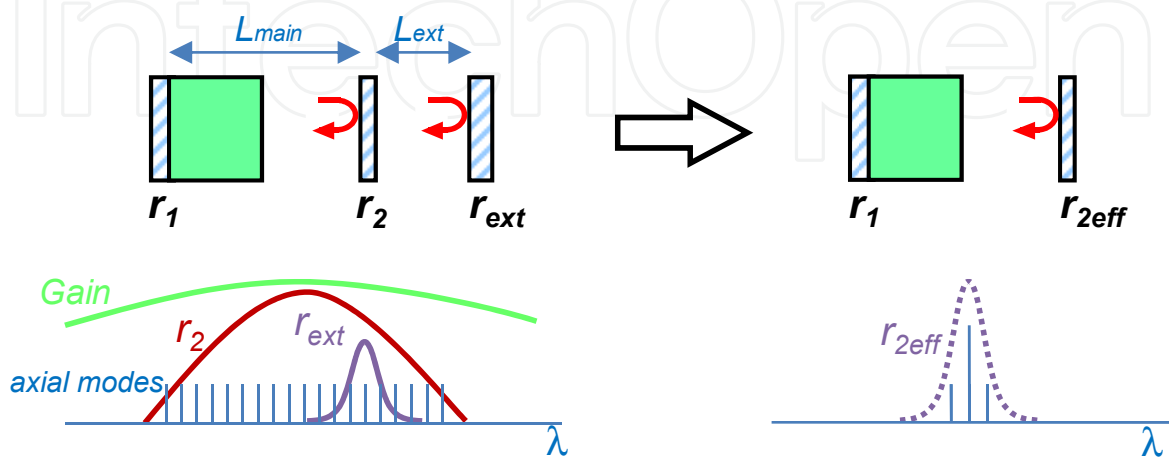

Fig. 7. External-cavity laser principle of operation.

The addition of an external reflector (r_{ext}) to a laser cavity (main cavity) modifies effectively the output electric field reflectivity of the main cavity (r_2) (Fig. 7) and then the three mirror cavity can be regarded as a two mirror cavity whit an output reflectivity r_{2eff}. This new r_{2eff} can be obtained from equation (6) (Tsunekane et al., 1998), where r_2, r_{ext} and r_{eff} are electric field reflection coefficients and τ_L round-trip time of the external cavity. As a result, the reflectivity is increased at some wavelengths.

$$r_{2eff} = \frac{r_2 + r_{ext} \exp(-j\omega\tau_L)}{1 + r_2 r_{ext} \exp(-j\omega\tau_L)} \tag{6}$$

As a consequence of an increased effective reflectivity the laser threshold is reduced and thus the intracavity power is also enhanced. If the external reflector permits wavelength tuning of its peak reflectivity and has narrow-band reflectivity (e.g. a diffraction grating) the emission linewidth is reduced and can be tuned. For a particular relation between the length of the main cavity and the length of the external cavity, the laser can be forced to emit in a single-axial mode (Tsunekane et al., 1998).

The most widely studied intracavity nonlinear frequency conversion process in Cr-doped colquiriites has been second-harmonic generation (SHG) in Cr:LiSAF lasers for tunable blue light generation (Balembois et al., 1992; Laperle et al., 1997; Eichenholz et al. 1998; Makio et al., 2000). In the following section we will widen the utility of Cr-doped colquiriites to new intracavity frequency conversion processes such as optical parametric oscillation (OPO) and difference frequency generation (DFG).

5. Examples of intra-cavity optical frequency conversion in Cr^{3+}:LiCAF lasers

In this section several optical frequency conversion devices based on Cr^{3+}-doped LiCaAlF$_6$ colquiriite plus a nonlinear optical crystal (NLOC) inside the laser cavity will be presented. Despite the converting systems described below uses a PPSLT crystal as a NLOC to operate in the 1500 – 1700 nm spectral region, they can be generalized to any nonlinear medium presenting transparency in the operation range. In each case, the system performance will be determined by the nonlinear and dispersive properties of the material employed depending on the application.

On one hand, the use of diode-pumped laser crystals as titanium sapphire or Cr^{3+}-doped colquiriite family (Cr^{3+}:LiSAF, Cr^{3+}:LiCAF and Cr^{3+}:LisGAF) appears as attractive options to operate since they provide a broad emission around 800 nm. However, the latter group presents the advantage of being directly pumped by commercial low-cost red diodes around 665 nm. Particularly, Cr:LiCAF arise as an optimum candidate due to its spectrally broad emission and homogeneous gain profile, which allow the generation of tunable narrow linewidth pump wavelengths from 720 nm to 840 nm approximately, and whose maximum power efficiency (emission cross-section) is located around 780 nm (Payne et al., 1988).

On the other hand, periodically poled ferroelectric materials have been widely employed for QPM interactions due to their high nonlinear coefficients and wide transparent range suitable for nonlinear processes from UV to mid-IR. In last years, periodically-poled stoichiometric lithium tantalate (PPSLT) has been paid much attention due to its resistance to photorefractive damage and laser damage (Buse et al., 2007; Skvortsov et al., 1993)

compared with other similar ferroelectric materials as congruent lithium tantalate (CLT) and congruent or stoichiometric lithium niobate (CLN or SLN, respectively). These properties should be specially taken into account in intracavity configurations, where powers confined in the nonlinear crystal can raise high values. However, the presence of MgO-doping in these compounds can help to mitigate optical degradation effects (Dolev et al., 2009).

In order to obtain efficient nonlinear interaction in the mentioned applications, quasi-phase matching (QPM) technique is employed in microstructured second order nonlinear crystals to correct the accumulated phase mismatching of the participating waves along propagation length ($\Delta k \neq 0$)). This way, the reciprocal vector $G = 2\pi/\Lambda$ introduced by a periodic structure with a period Λ compensates the wavevector mismatch $\Delta k = k_p - k_i - k_s - G = 0$ experimented by interacting waves as a consequence of the dispersion in nonlinear materials. Although QPM efficiency is lower than the efficiency obtained by perfect phase matching, the conversion efficiency can be compensated by accessing to larger nonlinear coefficients.

The emission spectrum of Cr:LiCAF is particularly well suited for the above mentioned processes. An optical parametric oscillator (OPO) operating near degeneracy can be constructed using the Cr:LiCAF laser radiation as the OPO pump wave, obtaining, therefore, two tunable wavelengths (signal and idler) in the 1550 nm optical communications band. Similarly, it tailors to the pump wave characteristics participating in wavelength conversion processes based on DFG in the vicinity of the degeneration in the same spectral band.

The present section is not aimed to obtain high lasing and frequency conversion efficiencies but to show the potential of these devices and techniques in several applications and address future improvements.

5.1 Optical parametric oscillation in a Cr^{3+}:LiCAF+PPSLT laser

Tunable dual-wavelength lasers are of particular interest for generation of tuneable terahertz (THz) radiation based on heterodyne mixing in photo-mixers, and for WDM channel conversion based on four wave mixing (FWM) in semiconductor optical amplifiers (SOAs). In this regard optical parametric oscillators are, by their nature, highly coherent dual-wavelength tunable optical sources (Nabors et al. 1990; Lee and Wong, 1993). In this section we present a doubly resonant intra-cavity pumped optical parametric oscillator (OPO) consisting of a Cr:LiCAF tunable laser and a periodically poled stoichiometric lithium tantalate (PPSLT) nonlinear crystal. The OPO radiation (signal + idler) can be tuned by means of any perturbation of the phase-matching condition (i.e. by either changing temperature or pump wavelength). Moreover, the laser cavity design permits tuning of the Cr:LiCAF radiation, which is used as pump wave for the parametric oscillation process.

The experimental set-up is shown schematically in Fig. 8. A 665 nm fiber coupled laser diode (LD) is used as optical pump for the Cr:LiCAF. Light from the laser diode is collimated (CL) and then focused (FL) into a 3% at. doped 1.5 mm long 3 mm diameter Cr:LiCAF crystal. The laser crystal was a-cut for polarized oscillation as required for efficient quasi-phase matching (d_{33}). One side of the Cr:LiCAF (M1) has dielectric coatings directly deposited for broadband high reflectivity for both 793±20 nm and 1586±100 nm spectral bands, and on the other side it is antireflection coated (AR) for both 800 nm and

1580 nm spectral bands, in an attempt to minimize intracavity loss. A periodically poled stoichiometric lithium tantalate (PPSLT) crystal is used as the non linear material to downconvert the pump wave (Cr:LiCAF laser) into two parametric waves (signal and idler). The crystal is 20 mm long with a 2x2 mm² cross sectional area, has anti-reflection (AR) coatings on both sides (AR@750-850 nm and AR@1500-1700 nm) and a grating period of 22.1 µm for type-0 QPM interaction. It is mounted in an oven for temperature control of the QPM condition. M1 and the output mirror (M2) form the main cavity for laser (Cr:LiCAF) and parametric (PPSLT) oscillation and it is 10 cm radius of curvature concave mirror and partially reflective coated for R≈98.5%@770-830 nm and R≈96.5%@1450-1650 nm.

The output from the main cavity is collimated (CL) and PPSLT OPO radiation is separated from Cr:LiCAF emission by means of a dichroic beam splitter (BS). Cr:LiCAF laser beam is then expanded using an anamorphic prism pair (4x) (APP) and fed back to the main cavity by means of a diffraction grating (G) (1200 lines/mm, blazing@750 nm) in a Littrow configuration. Beam expansion prior to diffraction grating improves spectral resolution of the diffraction grating. OPO pump wave tuning is therefore achieved through tilting of the diffraction grating. This allows OPO pump tuning, narrows the laser linewidth and increases the intracavity laser power (due to an increased effective reflectivity). Under the experimental conditions of Fig. 8, the OPO pump was tunable from 775 to 830 nm (Fig. 9.a).
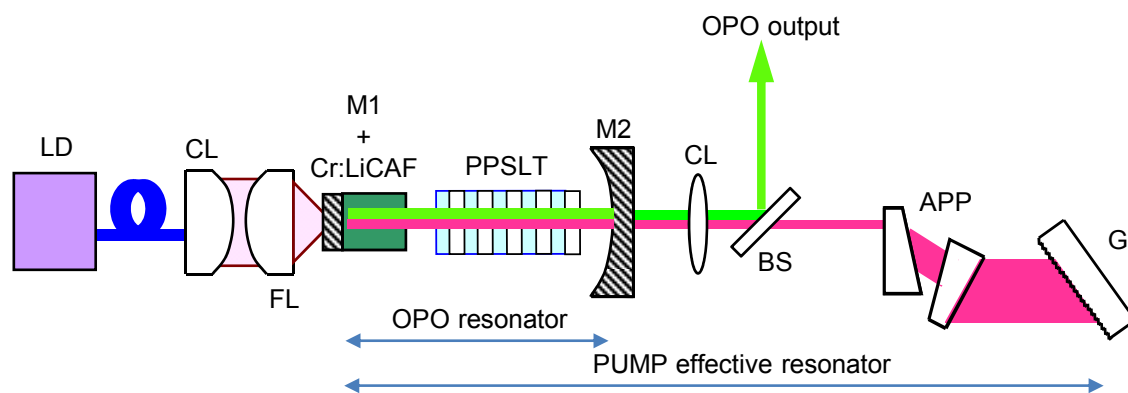

Fig. 8. Schematic of the intracavity pumped OPO experimental setup. LD: pump laser diode, CL: collimating lens, FL: focusing lens, M1: dielectric mirror directly deposited on the laser material input face, M2: concave mirror, BS: beam splitter, APP: anamorphic prism pair and G: ruled diffraction grating.

It is worth noting that there are two different cavities for Cr:LiCAF laser and OPO emission respectively. Parametric waves are resonated between M1 and M2 whereas Cr:LiCAF radiation is resonated between M1 and the effective reflectivity provided by M2 and the diffraction grating. If no external feedback is applied to the main cavity, Cr:LiCAF laser oscillates free-running with a relatively broad spectrum centered at 820 nm and more than 4 nm width, 650 mW of absorbed 665 nm power threshold and around 12% slope efficiency. This rather low slope efficiency is thought to be due to the high M² (beam quality factor) of the 665 nm pump system yielding a poor overlap between 665 nm pump beam and Cr:LiCAF laser cavity mode.

When optical feedback is applied, the Cr:LiCAF emission can be tuned and its spectrum is narrowed below 30 pm (optical spectrum analyzer limited). Fig. 9.b shows the relative

output power of the Cr:LiCAF laser at 792 nm for different operation conditions. If PPSLT is not inserted in the main cavity, the absorbed 665 nm pump power threshold is approximately 400 mW (Fig. 9.b squares) and a slope efficiency lower than 1% is obtained. This additional reduction of the slope efficiency is a consequence of an increased effective reflectivity of the output coupling when external feedback is added.
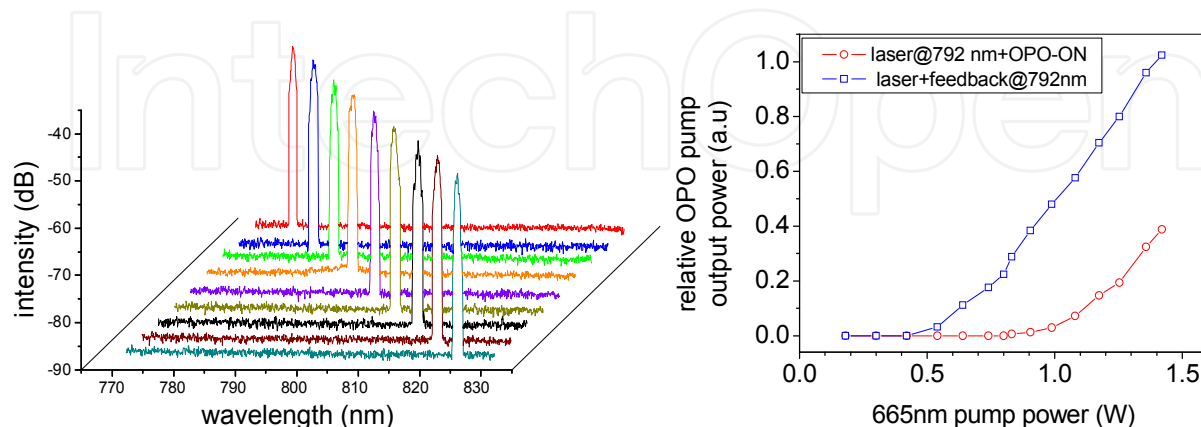

Fig. 9. Emission of the Cr:LiCAF laser: a) Wavelength tuning spectrum and b) output power under different operation conditions.

If the PPSLT crystal is placed with its extraordinary polarization parallel to the polarization of the laser (OPO ON, Fig. 9.b circles) and after adjusting the temperature of the non linear crystal, parametric generation takes place. As it can be observed, the 665 nm absorbed pump threshold power amounts to 750 mW and the slope efficiency is further reduced owing to the effect of residual reflectivity on faces of the PPSLT crystal and due to parametric generation. When parametric oscillation starts, it behaves as a wavelength dependant loss at the OPO pump wavelength (792 nm). Under this operation conditions the circulating Cr:LiCAF radiation is nearly 2 W but because of such OPO pump wavelength dependant loss, Cr:LiCAF 792 nm radiation coexists with 820 nm free-running radiation and, as the 665 nm power increases, both the fed back (792 nm) and the free-running (820 nm) radiation reach similar peak values. Thus, the available intra-cavity 792 nm power is sensitively below 2 W. As a result of this, a maximum OPO signal+idler output power of 10 mW is achieved. The OPO output power can be further enhanced by careful design of the mirror reflectivity around 800 nm, in order to fully suppress the free-running Cr:LiCAF oscillation (Stothard et al. 2009), and improving the beam quality factor (M^2) in order to improve the available intra-cavity OPO pump power.

After achieving parametric oscillation and starting from a degenerate OPO emission ($\omega_s \approx \omega_i$), the signal and idler waves were moved away from degeneracy by either temperature (Fig. 10. a) or pump wavelength (Fig. 10. b) tuning. Two examples of OPO emission spectrum for two different tuning conditions are shown in Fig. 10.c and in Fig. 10.d. Both tuning parameters allowed variable signal and idler wavelength separations between 0-250 nm (0-30 THz), limited by the reflectivity of the main cavity output mirror (M2) and the quasi-phase-matching condition. As it can be observed it follows the well-known parabolic relation between OPO output wavelength (signal and idler) and the tuning parameter (temperature or wavelength).

Because of operation near degeneracy (i.e. near the vertex of the parabola) the slope relating the change in OPO output wavelength to any tuning parameter is high and thus small changes in any tuning parameter produces a noticeable change in the OPO output wavelength (Lindsay et al., 1998; Wang et al. 2002), in contrast to OPOs working far from degeneracy. Therefore, if a fast signal-idler wavelength difference tuning is desired, pump wavelength tuning should be used instead of temperature tuning and, moreover, the faster the method employed for OPO pump wavelength tuning the faster will be the wavelength spacing between OPO signal an idler waves.
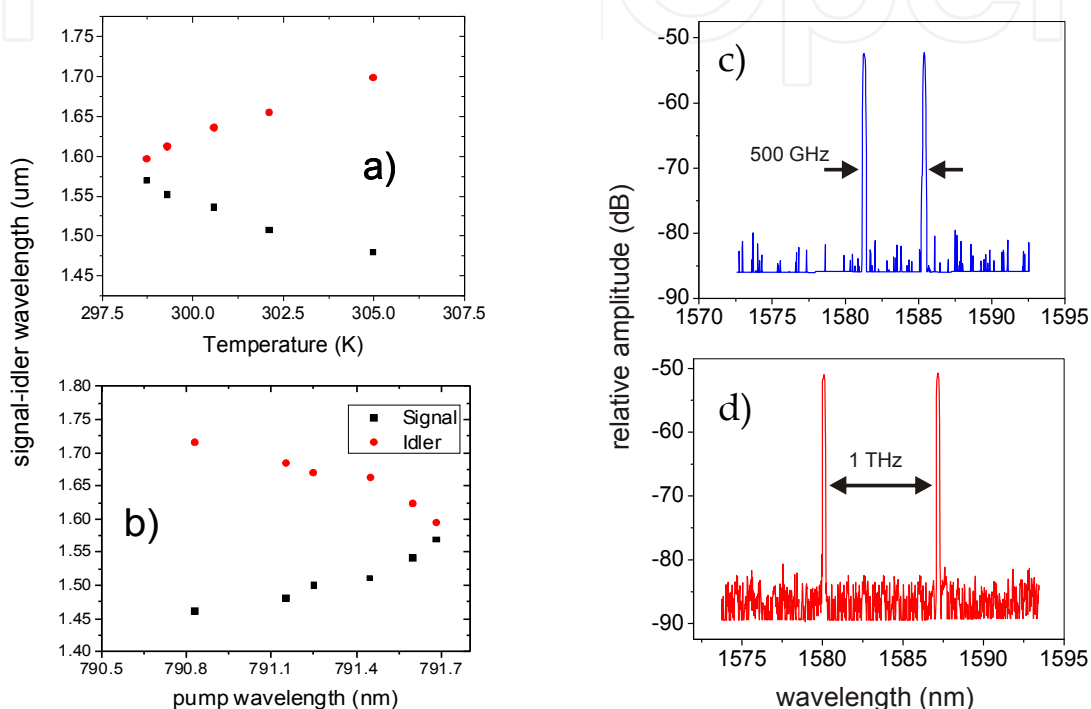
Fig. 10. Tuning of the dual-wavelength (signal+idler) OPO emission: a) temperature tuning, b) Cr:LiCAF laser tuning, c) and d) are examples of OPO emission spectrum with signal-idler frequency spacing of 0.5 THz and 1 THz respectively.

5.2 Difference frequency generation (DFG)

In recent years, the combination of the development of coherent sources based on nonlinear difference frequency generation (DFG) and the advances in the fabrication of nonlinear optical structures have led to cover new spectral regions and enhance spectral bands not efficiently developed in the infrared (IR) spectral region. In this context, continuous wave (CW) single-pass wavelength conversion of near and mid IR solid state lasers based on intracavity DFG in nonlinear media appears as an attractive approach to satisfy the present needs in optical communications (Yoo, 1996), sensing (Wysocki et al, 1994) or spectroscopy applications (Chen et al, 2006).

Difference frequency generation is produced when two waves, referred to as signal (at a frequency ω_s) and pump (an intense wave at a higher frequency ω_p), combine in a nonlinear medium to produce a new wave called idler at the difference frequency $\omega_i = \omega_p - \omega_s$ (after

energy conservation fulfillment). The wave-mixing process results from the nonlinear interaction among the optical waves and the nonlinear material characterized by its susceptibility $\chi^{(2)}$, as it is schematically represented in Fig. 11.

Wavelength conversion processes are commonly characterized by the conversion efficiency defined in equation (3). But in practice, interacting waves have some finite spatial extent in the plane transverse to the direction of propagation, so the spatial confinement is taken into account through the Boyd-Kleinman factor h in such equation. This factor collects the effects produced by the interaction of focused gaussian beams in nonlinear media (Boyd and Kleinman, 1968) depending on the material properties as walk-off and absorption, the phase mismatching, and the focusing conditions experimented by the participating waves. A trade-off between the confinement and the interaction length is required to guarantee the optimal overlapping between modes along the nonlinear, and thus enhancing the conversion efficiency. In this sense, type-0 QPM interactions, in which all participating waves have identical polarization (extraordinary), avoids the presence of walk-off and enables the access to the largest coefficient d_{33} in the second-order nonlinear tensor, leading to more efficient processes.
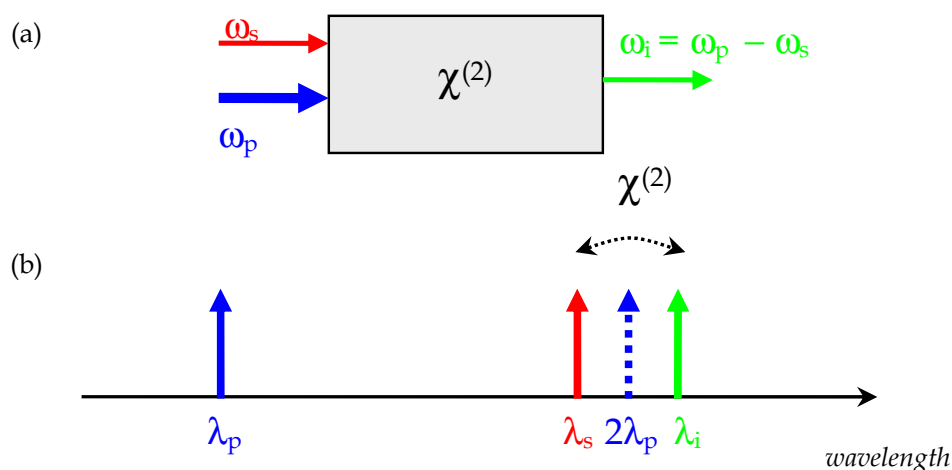

Fig. 11. Difference frequency generation (a) Diagram of the wave generation ω_i from the mixing of an intense pump wave ω_p and a weak wave ω_s in a nonlinear medium $\chi^{(2)}$. (b) Spectral allocation of components involved in the wavelength conversion process.

Since the nonlinear mixing is proportional to the pump intensity, the efficiency of continuous-wave (CW) optical frequency generation can be increased by placing the nonlinear crystal inside the resonant cavity where the pump wave is generated. Then, the power level of the converted wave can be improved some magnitude orders in comparison with the provided by external processes. This way, the efficiency of DFG processes based on crystals with low nonlinear coefficient can be also compensated by the presence of high intracavity pump power. On the other hand, the conversion efficiency also describes sum and second harmonic generation similarly to that obtained in DFG. However, unlike the formers it is to be noted that when DFG occurs, not only idler photons are generated, but also new signal photons are created from the decomposition of pump photons as a consequence of the energy conservation fulfilment, and thus providing the amplification at both signal and idler wavelengths.

Unlike other conversion techniques, DFG preserves both phase and amplitude features of the incoming signal, providing a strict degree of transparency. In addition to this, DFG enables the conversion of multiple input wavelengths simultaneously what makes it an ideal technology to be exploited in the next generation of optical converters in communication applications (Yoo, 1996). This performance is achieved thanks to the wide spectral bandwidth experimented by the signal and idler waves in QPM devices (Fejer et al, 1992), which also can be extended for broadband conversion as it is seen in the next section. In order to show the potential of this technique, a flexible and versatile wavelength converting system for optical telecom signals based on single-pass DFG in a PPSLT crystal placed inside a CW tuneable solid-state laser is described in the following lines. In such applications, wavelength conversion usually covers the spectral region ranging from 1500 to 1700 nm, so the generation of a pump wave around 800 nm is required.

On the left of Fig.12 it is represented the theoretical QPM tuning curves in 1500-1700 nm band (for both signal and idler waves) as a function of the PPSLT temperature and for different pump wavelengths (792, 793 and 794 nm) from Sellmeier equations (Bruner et al., 2003). Furthermore, conversion efficiency curves for the operation temperatures (28, 41 and 53ºC) are shown in detail on the right side from extracted slides. So, given a fixed external signal, it can be seen how idler wave is shift to higher wavelengths (up to 8 nm) as pump wavelength is increased.
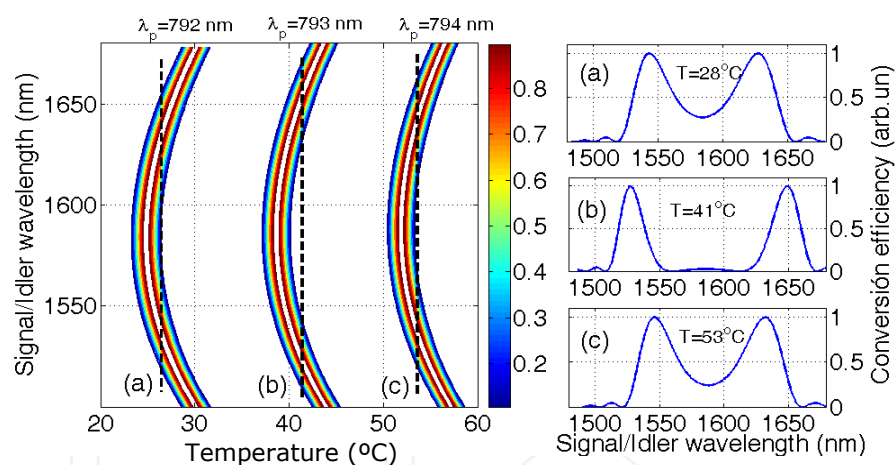

Fig. 12. QPM tuning curves for the PPSLT crystal (*L*=20 mm and Λ=22.1µm) for different operation temperatures: (a) T=28ºC, (b) T=41ºC, (c) T=53ºC.

The experimental set-up of the wavelength converting system is schematically shown in Fig. 13. The laser cavity consists of a two-arm V-folded main cavity defined by three mirrors (M1, M2 and M3). A 3 mm long a-cut end-pumped Cr³⁺:LiCAF crystal rod doped with 3 at.% of chromium, and with a 3 mm of diameter is employed as the gain medium. Mirror M1 is coated directly on the input facet of Cr³⁺:LiCAF crystal whereas mirrors M2 and M3 are plano-concave spherical mirrors arranged in a confocal configuration to produce a beam waist in the middle of the second arm, where the center of the PPSLT is placed. Thus, tightly confined signal and pump beams can be easily made to overlap in a collinear interaction thus improving the conversion efficiency. The PPSLT is 20 mm long with a 2 × 2 mm² cross sectional area and a grating period of 22.1 µm, which is mounted in an oven for temperature

control of QPM conditions and to reduce potential photorefractive effects. Self-injection-locking is provided by an external coupled cavity based on a Littrow-mounted ruled diffraction grating which allows for tuneable oscillation around 792±8 nm with a spectral width narrower than 1 nm. Then, the pump wave is collinearly mixed with a signal generated from a tunable multi-wavelength erbium doped fiber laser whose output, comprised between 1530 and 1570 nm, is amplified and partially polarized prior to its introduction into the laser cavity in order to enhance the conversion efficiency.
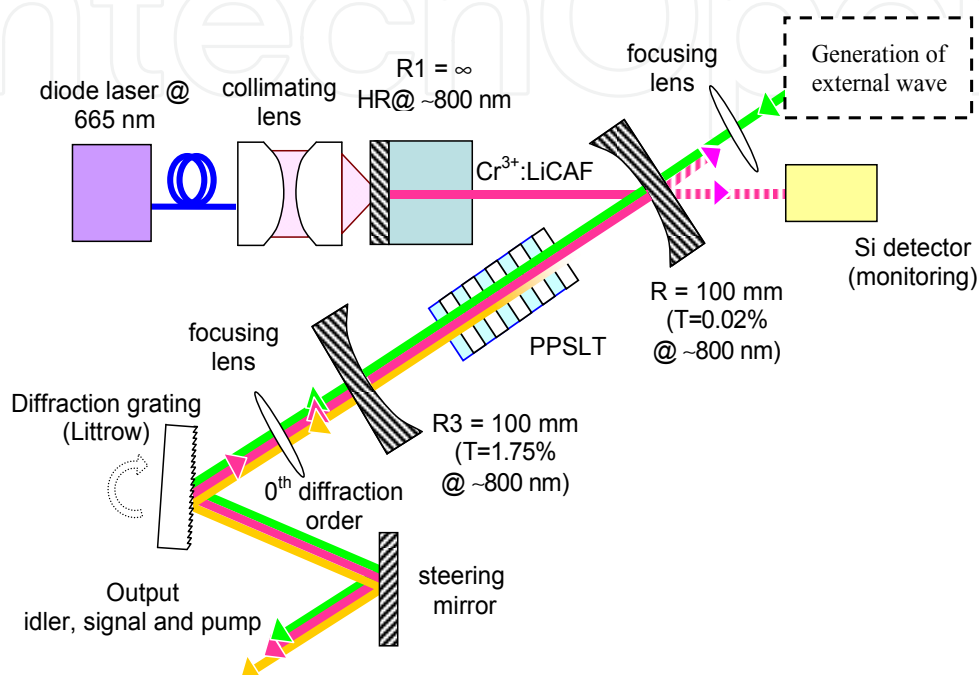
Fig. 13. Experimental setup for DFG processes.

Simultaneous multi-wavelength conversion is represented in Figure 14 for several arbitrary wavelengths (channels) and combinations at 1547, 1551 and 1555 nm. A pump wavelength at 794 nm (represented in Fig. 14 as OSA second order as a spectral reference) is used in the mixing process when the PPSLT crystal is heated up to 53°C to satisfy QPM condition. Idler waves generated at ~1631, 1627 and 1623 nm, comprising a spectral range of 7.8 nm where no more than a 4% of penalty with regard to the maximum QPM theoretical conversion efficiency is experimented, so in this case QPM condition does not suppose any limiting factor. The spectral allocation of the converted spectrum can be tuned by tilting the grating thanks to the characteristic broadband gain of Cr^{3+}:LiCAF (Payne et al., 1988) and by temperature adjustment of the PPSLT crystal to satisfy the required QPM condition.

Although the experimental conditions available restricted the laser operation to only 1.5 times above threshold with a modest intra-cavity power around 2 W, improving the laser design to approach the typical performances achievable with diode-pumped Cr3+:LiCAF lasers (Demirbas et al., 2009) should lead to high conversion efficiencies, even in excess of 100% if the laser is carefully designed to achieve net parametric gain at reasonably feasible values of intra-cavity power. Due to the nature of the DFG process, the conversion efficiency becomes independent of the input signal power and it is therefore suitable for weak input signals.
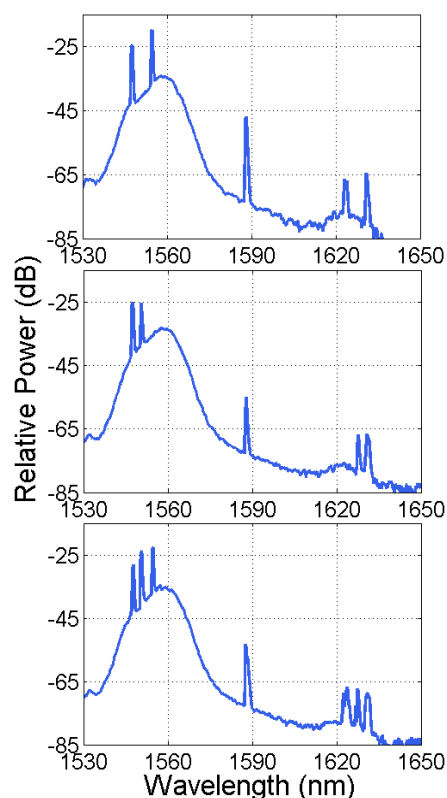
Fig. 14. Simultaneous wavelength conversion.

5.3 Broadband conversion

The emergence of applications which require the use of broad spectral regions where there are not optical sources or they have not been efficiently developed have made grow the interest in broadband wavelength conversion techniques recently. The availability of broadband optical sources is interesting in a variety of applications which ranges from wavelength division multiplexing (WDM), passive optical networks (PON) based on spectral slicing techniques (Jung et al., 1998), interferometric sensors (Wysocki et al., 1994), and biomedicine such as optical coherence tomography (Schmitt, 1999).

For this aim, the intracavity broadband conversion based on DFG processes in QPM devices can be an attractive and effective alternative to those techniques based on the generation of nonlinear processes such as cross-gain or cross-phase modulation (XPG, XPM) and four wave mixing (FWM) in semiconductor optical amplifiers (SOAs) following interferometric arrangements and highly nonlinear fiber configurations (Bilenca et al., 2003). This scheme exploits not only the advantages of active conversion, but also the wide spectral acceptance of the signal/idler waves in periodically poled ferroelectric crystals. Furthermore, due to the DFG nature, the spectrum of the converted wave undergoes the spectral inversion with regard to the pump wave while the spectral fidelity is preserved. This opens up a way for wavelength conversion of weak broadband sources since no threshold is required, as it is derived from equation (3).

Given a broadband input signal with a bandwidth of B and centered at ω_s, the allocation of the targeted idler spectrum depends on the spectral position of the pump wave ω_p. In this

way, a proper choice of the pump wavelength is required to satisfy the quasi-phase matching condition imposed by the nonlinear crystal features, and then, different performances can be obtained; a broadband signal can be displaced to a spectral region where no coherent source is available (Fig. 15.a), a spectrally variable bandwidth up to 2B can be achieved by tuning the pump wave so that $\omega_p/2$ falls in the vicinity of the spectral components delimiting the signal band (Fig. 15.b), and spectral shaping from total or partial overlap of involved spectra provided by QPM structures (Fig. 15.c). In this case, domain engineering in nonlinear ferroelectric crystals could provide particular QPM tuning curves that lead to dynamic and flexible resultant responses depending on the overlapping between the signal and idler spectra.
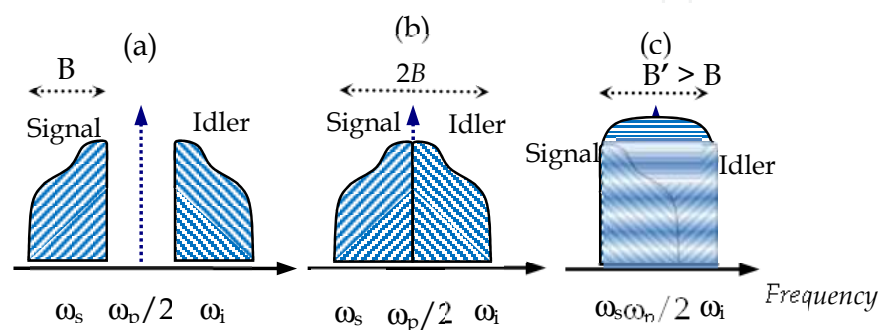
Fig. 15. Broadband conversion operation modes based on DFG from a pump wave at ωp and a broadband signal wave centered at ωs with a spectral bandwidth of B.

Intra-cavity assisted broadband wavelength conversion for an incoherent continuous-wave input source (ASE, amplified spontaneous emission source) has been recently demonstrated in the spectral region around 1535-1635 nm (Torregrosa et al., 2011). Following an experimental setup similar to that proposed in the previous section, Fig. 16 shows the broadband conversion results when an ASE source based on a diode-pumped Erbium-doped fiber is used. The output of the ASE source, which is spectrally extended from 1530-1565 nm, is collinearly mixed with a pump wave tuned at 794 nm (represented as OSA second order as a spectral reference) in a PPSLT crystal at 53°C. As a result of the mixing process, a broadband idler ranging from 1605 to 1635 nm is generated, in which spectral inversion is revealed clearly. Furthermore, a shift up to 8 nm of the broadband spectrum is achieved by tuning the pump wavelength accordingly with the crystal temperature to satisfy QPM condition, as it is shown in the inset of Fig. 16.
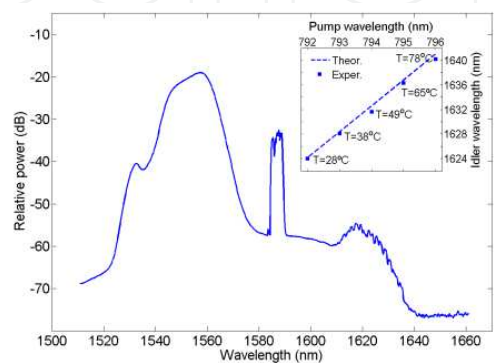

Fig. 16. Power spectra of the measured broadband conversion process

Despite the very limited experimental conditions available with a modest intra-cavity power laser operating only 1.5 times above threshold, it is shown that improving the laser design should lead to a high conversion efficiency (even in excess of 100%). Fortunately, the efficiency can be improved by increasing the intracavity pump power since the efficiency is proportional to the pump wave intensity according to equation (3). Thus, the converting scheme here described emerges as an attractive and versatile tool for extending the availability of outstanding ASE sources to spectral regions other than their natural emission spectrum using a simple periodically poled crystal.

6. Conclusions and future work

Spectral caracteristics of solid-state lasers based on Cr-doped colquiriites allow to select the emission wavelength from a wide gain spectrum, and can be pumped by comercially available laser diodes. Owing to its spectral emission in the vecinity of 800 nm, they can be employed in intracavity nonlinear conversion to generate radiation in the 1500-1700 nm spectral band where DFG and OPO have not been studied in detail so far, in contrast to the SHG case.

Intracavity wavelength conversion is characterized by presenting conversion efficiencies typically two orders of magnitude greater than those offered by external processes. However, the results obtained present reduced conversion efficiencies due to the restrictions imposed by experimental conditions available, such as the limited 665 nm pump power, and mainly, the inefficient adaptation between the 665 nm pump mode and laser oscillation mode as a result of the poor quality of the former ($M^2>>1$). From the spectral point of view, the performance obtained reveals the advantages and versatility to operate in a huge variety of applications.

Since QPM is associated to the use of ferroelectric crystals, such as lithium or tantalate niobate, by strategic domain distributions it is possible to provide QPM tuning responses associated to particular applications in addition to the ability to operate in regimes not accessible to conventional birefringently phasematched media.

Finally, although the experimental setups of the converting systems here presented appear as bulky schemes (as a result of the space required for handling, measuring and characterizing the system performance), the underlying technology to diode pumped solid-state lasers enables the implementation of compact devices by taking advantage of the microchip laser technology (Zayhowski, 1997). A further compactness could be achieved by doping with Cr³⁺ ions into the nonlinear medium, as it has been previously demonstrated in periodically poled ferroelectric crystals (Capmany et al., 2000). This way, the laser oscillator and the nonlinear optical converter would be integrated in the same crystal, leading to promising laser schemes as self-frequency converters.

7. References

Balembois, F.; Georges, P.; Salin, F.; Roger, G. and Brun, A. (1992), Tunable blue light source by intracavity frequency doubling of a Cr-doped LiSrAlF6 laser. *Applied Physics Letters.*, Vol. 61, No. 20, pp. 2381–2383. ISSN: 0946- 2171 (Print) ISSN: 1432-0649 (Online).

Belmonte M., Skettrup T.; Pedersen C.; (1999), Frequency doubling in LiNbO3 using temperature-dependent QPM, *Journal of Optics A-Pure And Applied Optics*, Vol. 1, No. 1, pp. 60-63, ISSN (printed): 1464-4258. ISSN (electronic): 1741-3567.

Bilenca A.; Alizon R.; Mikhelashhvili V.; Dahan D.; Eisenstein G.; Rchwertberger R.; Gold D.; Reithmaier J. P. and Forchel A., (2003), Broad-Band Wavelength Conversion Based on Cross-Gain Modulation and Four-Wave Mixing in InAs-InP Quantum-Dash Semiconductor Optical Amplifiers Operating at 1550 nm, *IEEE Photonics Technology Letters*, Vol. 15, No. 4, pp. 563-565, ISSN: 1041-1135.

Boyd G. D. and Kleinman, D. A., (1968), Parametric Interaction of Focused Gaussian Light Beams, *Journal of Applied Physics*, Vol. 39, No. 8, pp. 3597-3641, Print: ISSN 0021-8979, Online: ISSN 1089-7550.

Bruner A.; Eger D.; Oron M. B.; Blau P.; Katz M. and Ruschin S., (2003), Temperature-dependent Sellmeier equation for the refractive index of stoichiometric lithium tantalate, *Optics Letters*, Vol. 28, pp. 194-196, ISSN: 0146-9592 (print), ISSN: 1539-4794 (online).

Buse K.; Imbrock J.; Krätzig E. and Peithmann K., (2007), Photorefractive Effects in LiNbO3 and LiTaO3, In: *Photorefractive Materials and Their Applications 2*, P. Günter, J. P. Huignard, pp. 83-126, Ed. Springer, ISBN 978-0387-33924-5, USA.

Capmany, J.; Montoya, E.; Bermúdez, V.; Callejo, D.; Diéguez, E. and Bausá, L. E., (2000), Self-frequency doubling in Yb3+ doped periodically poled LiNbO3:MgO bulk crystal, *Applied Physics Letters*, Vol. 76, No. 11, pp. 1374-1376, ISSN 0003-6951 (print), ISSN 1077-3118 (online)

Chen W.; Cousin J.; Poullet E.; Boucher D.; Xiaoming G.; Sigrist M.W. and Tittel F.K., (2006), Laser Difference-Frequency Generation in the Mid-Infrared and Applications to High-Resolution Molecular Spectroscopy and Trace Gas Detection, *Joint 31st International Conference on Infrared Millimeter Waves and 14th International Conference on Terahertz Electronics*, 2006. pp. 583.

Demirbas U.; Li D.; Birge J. R.; Sennaroglu A.; Petrich G. S.; Kolodziejski L. A.; Kärtner F. X. and Fujimoto J. G., (2009), Low-cost, singlemode diode-pumped Cr:colquiriite lasers, *Optics Express*, Vol. 17, No. 16, pp. 14374–14388, ISSN: 1094-4087.

Dolev I.; Ganany-Padowicz A.; Gayer O.; Arie A.; Mangin J. and Gadret G. (2009). Linear and nonlinear optical properties of MgO:LiTaO3, *Applied Physics B*, Vol. 96, No 2-3, pp. 423-432. ISSN: 0946- 2171 (Print) ISSN: 1432-0649 (Online).

Eichenholz, J. M. and Richardson, M. (1998). Measurement of Thermal Lensing in Cr-Doped Colquiriites, *IEEE Journal of Quantum Electronics*, Vol. 34, No. 5, pp. 910-919, ISSN: 0018-9197.

Eichenholz, J. M.; Richardson, M. and Mizell, G. (1998), Diode-pumped, frequency doubled LiSAF microlaser. *Optics Communications*, Vol. 153, No. 5, pp. 263–266. ISSN: 0030-4018.

Fejer M. M.; Magel G. A.; Jundt D. H and Byer R. L., (1992) Quasi-phase-matched second harmonic generation: tuning and tolerances, *IEEE Journal of Quantum Electronics*, Vol. 28, No. 11, pp. 2631–2654 (1992), ISSN: 0018-9197.

Fernandez-Pousa, C. R. and Capmany, J., (2005), Dammann grating design of domain-engineered lithium niobate for equalized wavelength conversion grids, *IEEE Photonics Technology Letters*, Vol. 17, No. 5, pp. 1037-1039, ISSN: 1041-1135.

Jung D. K.; Shin S. K.; Lee C. H. and Chung Y. C., (1998), Wavelength-division-multiplexed passive optical network based on spectrum-slicing techniques, *IEEE Photonics Technology Letters*, Vol. 10, No. 9, pp. 1334-1336, ISSN: 1041-1135.

Laperle, P.; Snell, K. J.; Chandonnet, A.; Galarneau, P. and Vallée, R. (1997), Tunable diode-pumped and frequency-doubled Cr:LiSAF lasers. *Applied Optics*, Vol. 36, No. 21, 5053–5057. ISSN: 1559-128X (print), ISSN: 2155-3165 (online).

Lee, D. and Wong, N. C. (1993), Stabilization and tuning of a doubly resonant optical parametric oscillator, *Journal of the Optical Society of America B,* Vol. 10, No. 9, pp. 1659-1667, ISSN: 0740-3224 (print), ISSN: 1520-8540 (online).

Lindsay, I. D.; Turnbull, G. A.; Dunn, M. H. and Ebrahimzadeh, M. (1998). Doubly resonant continuous-wave optical parametric oscillator pumped by a single-mode diode laser, *Optics Letters*, Vol. 23, No. 24, pp. 1889-1891, ISSN: 0146-9592 (print), ISSN: 1539-4794 (online).

Liu, H; Zhu, YY; Zhu, SN; Zhang, C; Ming, NB, (2001), Aperiodic optical superlattices engineered for optical frequency conversion, *Applied Physics Letters*, Vol. 79, No. 6, pp. 728-730, ISSN 0003-6951 (print), ISSN 1077-3118 (online).

Nabors, C. D.; Yang, S. T.; Day, T.; Byer, R. L. (1990), Coherence properties of a doubly resonant monolithic optical parametric oscillator, *Journal of the Optical Society of America B,* Vol. 7, No. 5, pp. 815-820, ISSN: 0740-3224 (print), ISSN: 1520-8540 (online).

Maiman, T. H. (1960). Stimulated Optical Radiation in Ruby. *Nature*, Vol. 187, pp. 493-494. ISSN: 0028-0836

Makio, S.; Miyai, T.; Sato, M. and Sasaki, T. (2000) 67 mW Continuous-wave blue light generation by intracavity frequency doubling of a diode pumped Cr:LiSrAlF6 laser. *Japanese Journal of Applied Physics*, Vol. 39, pp. 6539–6541, ISSN: 0021-4922 (print), ISSN: 1347-4065.

Payne, S. E.; Chase, L. L. ; Newkirk, H. W.; Smith, L. K. and Kupke W. F., (1988), LiCaAlF6:Cr3+: A promising New Solid Satate Laser Material, *IEEE Journal of Quantum Electronics*, Vol. 24, No. 11, pp. 2243-2252, ISSN: 0018-9197.

Payne, S.; Chase, L.; Smith, L.; Kway, W. and Newkirk, H. (1989). Laser performance of LiSrAlF6:Cr3+, *Journal of Applied Physics*, Vol. 66, No. 66, pp. 1051-1056. , Print: ISSN 0021-8979, Online: ISSN 1089-7550.

Schmitt J. M., (1999). Optical Coherence Tomography (OCT): A Review, *IEEE Journal of Selected Topics in Quantum Electronics*, Vol. 5, No. 5, pp. 1205-1215, ISSN: 1077-260X.

Skvortsov, L. A. and Stepantsov, E. S. (1993), Laser damage resistance of a lithium niobate-tantalate bicrystal system, *Quantum Electronics*, Vol. 23, No. 11, pp. 981-982. ISSN 1063-7818 (Print). ISSN 1468-4799 (Online).

Smith, R. G., (1970), Theory of Intra-cavity Optical Second-Harmonic Generation, *IEEE Journal of Quantum Electronics*, Vol. 6, No. 4, pp. 215-223, ISSN: 0018-9197.

Smith, L.; Payne, S.; Kway, W.; Chase, L.; Chai, B. (1992). Investigation of the laser properties of Cr3+:LiSrGaF6, *IEEE Journal of Quantum Electronics*, Vol. 28, No. 11, pp. 2612 – 2618, ISSN: 1077-260X.

Stothard, D. J.; Hopkins, J-M.; Burns, D. and Dunn, M. H. (2009). Stable, continuous-wave, intracavity, optical parametric oscillator pumped by a semiconductor disk laser (VECSEL), *Optics Express*, Vol. 17, No. 13, pp. 10648-10658, ISSN: 1094-4087.

Torregrosa, A. J. ; Maestre, H. ; Fernández-Pousa, C. R. and Capmany J., (2008) Electro-Optic Reconfiguration of Quasi-Phase Matching in a Dammann Domain Grating for WDM Applications, *Conference on Lasers and Electro-Optics/Quantum Electronics and Laser Science Conference and Photonic Applications Systems Technologies*, paper CWC1.

Torregrosa, A. J. ; Maestre, H. and Capmany, J., (2011) Wavelength conversion of a broadband ASE source based on intra-cavity difference-frequency-mixing in a Cr3+:LiCAF-PPSLT laser, *The European Conference on Lasers and Electro-Optics (CLEO/Europe)*, paper CD_P23.

Tsunekane, M.; Ihara, M.; Taguchi, N. and Inaba, H. (1998). Analysis and Design of Widely Tunable Diode-Pumped Cr:LiSAF Lasers with External Grating Feedback, *IEEE Journal of Quantum Electronics*, Vol. 34, No. 7, pp. 1288-1296, ISSN: 1077-260X.

Wang, H.; Ma, Y.; Zhai, Z.; Gao, J.; Xie, C. and Peng, K. (2002). Tunable Continuous-Wave Doubly Resonant Optical Parametric Oscillator by Use of a Semimonolithic KTP Crystal, *Applied Optics*, Vol. 41, No. 6, pp. 1124-1127. ISSN (printed): 1464-4258. ISSN (electronic): 1741-3567.

Wysocki P. F. ; Digonnet M.J.F. ; Kim B. Y. ; Shaw H. J. (1994), Characteristics of Erbium-doped Superfluorescent Fiber Sources for Interferometric Sensor Applications, *IEEE Journal of Ligthwave Technology*, Vol. 12, No. 3, pp.550-567, ISSN: 0733-8724.

Xu F. ; Liao J. ; Wang Q. ; Du J. ; Xu Q. ; Liu S. ; He J.L. ; Wang H.T. ; Ming N.B. (2003), Electro-optically controlled efficiencies in a QPM coupled parametric process, *Applied Physics B: Lasers and Optics*, Vol. 76, No. 7, pp. 797-800, ISSN: 0946- 2171 (print version) ISSN: 1432-0649 (electronic version).

Yoo S.J.B., (1996) Wavelength conversion technologies for WDM network applications, *IEEE Journal of Ligthwave Technology*, Vol.14, No. 6, pp. 955-966, ISSN: 0733-8724.

Zayhowski, J. J. (1997), Microchip optical parametric oscillators, *IEEE Photonics Technology Letters*, Nol.9, No.7, pp.925-927, ISSN: 1041-1135.
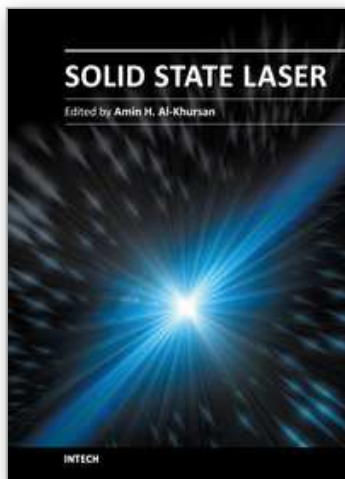
Solid State Laser

Edited by Prof. Amin Al-Khursan

ISBN 978-953-51-0086-7

Hard cover, 252 pages

Publisher InTech

Published online 17, February, 2012

Published in print edition February, 2012

This book deals with theoretical and experimental aspects of solid-state lasers, including optimum waveguide design of end pumped and diode pumped lasers. Nonlinearity, including the nonlinear conversion, up frequency conversion and chirped pulse oscillators are discussed. Some new rare-earth-doped lasers, including double borate and halide crystals, and feedback in quantum dot semiconductor nanostructures are included.

INTECH

open science | open minds